Clays and Clay Minerals, Vol. 56, No. 6, 622–632, 2008.

MINERALOGY, GEOCHEMISTRY, AND DIAGENESIS OF CLINOPTILOLITE TUFFS (MIOCENE) IN THE CENTRAL SIMAV GRABEN, WESTERN TURKEY

RUBEN SNELLINGS*, TOM VAN HAREN, LIEVEN MACHIELS, GILLES MERTENS, NOËL VANDENBERGHE, AND JAN ELSEN

Department of Earth and Environmental Sciences, Catholic University of Leuven, B-3001 Leuven, Belgium

Abstract—Miocene rifting and associated rhyolitic (K-rich) volcanism resulted in the deposition of pyroclastic material in the central Simav graben, near Karacaderbent, Turkey. The pyroclastics were deposited in a lacustrine environment, altered to clinoptilolite-rich tuffs and cross-cut by several transform faults along which hydrothermal fluids circulated. Petrography and quantitative phase analysis by X-ray diffraction show that the Karacaderbent tuff consists mainly of the diagenetic products clinoptilolite, opal CT, smectite, and celadonite. Electron microprobe analyses and cation exchange capacity (CEC) measurements confirm the predominance of K-rich clinoptilolite. Near fault zones, clinoptilolite was replaced by authigenic opal CT and alkali feldspar, and the remaining clinoptilolite was enriched in Na. Silicification around fault zones was confirmed by X-ray fluorescence. Zeolitization of K-rich rhyolitic starting materials took place under mildly alkaline, low-salinity conditions, probably in a closed hydrologic system. The subsequent hydrothermal alteration along faults had only a minor impact. The homogeneous nature, large (74–87 wt.%) clinoptilolite content, large CEC, and K-rich composition of the deposit favor exploitation of this material for applications in agriculture, horticulture, and waste-water purification; as feed additives; and as pozzolans for cement production.

Key Words—Clinoptilolite, Diagenesis, Karacaderbent, Kizilbük Formation, Simav Graben, Tuff, Turkey, Western Anatolia, Zeolites.

INTRODUCTION

During the Neogene in western Turkey, extensional N–S tectonics resulted in the formation of a large number of northeast- and northwest-trending grabens (Bozkurt, 2001). The sedimentary record in the Neogene grabens shows the deposition of volcano-sedimentary sequences consisting of detrital sediments originating from the surrounding basement, products of K-rich calc-alkaline volcanism, carbonates, and in several cases evaporites formed in arid lacustrine environments (Purvis and Robertson, 2005). In many grabens and basins, pumiceous and vitric pyroclastic deposits were diagenetically altered and created a zeolite province of regional extent (Gündogdu *et al.*, 1996).

The most important zeolite occurrences in western Anatolia and surrounding regions were formed in saline-alkaline lakes. They are associated with borates, carbonates, K-feldspar, and clay minerals in the Bigadiç, Kirka, and Emet basins (Helvaci *et al.*, 1993; Gündogdu *et al.*, 1996) and in the Karlovassi basin on the Island of Samos, Greece (Stamatakis, 1989). In Beypazari, zeolites are found with soda minerals, carbonates, K-feldspar, and clay minerals (Helvaci *et al.*, 1993). In Gördes, a commercially exploited deposit, zeolites were described in association with carbonate, K-feldspar, and clay minerals (Esenli and Sirkecioglu, 2005). Common zeolites and associated authigenic silicate minerals in western Anatolia are clinoptilolite, heulandite, analcime, mordenite, erionite, phillipsite, opal CT, K-feldspar, quartz, and smectite.

In general, the zeolitization environment is in many cases a debatable issue as sedimentary zeolites can occur in a wide range of geologic environments or hydrogeologic systems (Sheppard and Hay, 2001). In the Simav graben, the geologic setting indicates that zeolites could have formed either in a high-temperature hydrothermal system or in low-temperature open to closed hydrologic systems (Gündogdu *et al.*, 1996; Oygür and Erler, 1999; Mutlu *et al.*, 2005).

Renewed exploration and exploitation of zeolites has been prompted by recent increased interest in natural zeolite applications for agriculture and water treatment, and for pozzolanic or for supplementary materials in cement production. For appropriate selection of applications, a profound knowledge of deposit properties is needed (Mumpton, 1999). Therefore, the aim of the present study was to characterize the mineralogy and geochemistry of the diagenetically altered tuffaceous rocks in the central Simav graben near Karacaderbent and to discuss the diagenetic alteration environment of the zeolite facies.

GEOLOGIC SETTING

The study area is situated in the central part of the Simav graben, 20 km east of Simav, near the village of Karacaderbent, western Anatolia, Turkey, 4 km west of

* E-mail address of corresponding author:
ruben.snellings@ees.kuleuven.be
DOI: 10.1346/CCMN.2008.0560603

the Saphane alunite deposit (Figure 1). The WNW–ESE-directed Simav graben developed as a consequence of extensional rifting in the neo-tectonic period (Miocene to Pliocene) along the pre-existing dextral strike-slip Simav fault which was installed during the compressional regime of the paleo-tectonic period (Upper Cretaceous to Paleocene) (Oygür and Erler, 1999). Several Au-Hg-Sb and alunite epithermal ore deposits are related to the Simav graben (Mutlu *et al.*, 2005), and occur along N–S transfer faults formed during the neo-tectonic period. Recent epithermal activity is demonstrated through the presence of hot springs and sinter precipitation along the graben (Oygür and Erler, 1999).

The Miocene volcano-sedimentary succession in the Simav graben rests unconformably on Paleozoic metamorphosed and Mesozoic ophiolites and carbonates associated with the Izmir-Ankara suture (Figure 1). The Middle Miocene volcano-sedimentary sequence graben infill up to 600 m thick is called the Kizilbük formation and consists of yellow-brownish to gray-greenish sandstones, claystones, and white tuff lenses deposited in a lacustrine environment (Mutlu *et al.*, 2005). Zeolite-facies alteration of several white tuff lenses took place. The Kizilbük formation is reported as transitional to the overlying rhyolitic Middle Miocene Civanadag tuff. The Akdag volcanite consists of light-gray lava flows of rhyodacitic composition and occurs lateral to the Civanadag tuff (Mutlu *et al.*, 2005). K-Ar radiometric dating gave a Middle-Miocene age for the Akdag volcanite (14.6 Ma; Seyitoglu *et al.*, 1997).

The investigated zeolite deposit occurs as a tuff lens in the lacustrine Kizilbük formation and will be referred to henceforth as the 'Karacaderbent tuff.' North of the deposit, the Akdag volcanics overly the Kizilbük formation. Due to post-depositional deformation along E–W normal and several NW–SE transform faults, the tuff lens is segmented into five blocks (Figure 2). The faults contain fault breccia and silica sinter. Based on field observations, the north face of the deposit was identified as an E–W-oriented normal fault system with evidence of brecciation and focused fluid flow that resulted in local silicification. The extent of the silicification zone increases toward the intersection of the fault systems from ~0.5 m to ~15 m. A diagenetic alteration overprint that could be traced along the fault showed alternations of cm-wide blue and ochre layers parallel to the fault.

Each unit is predominantly built up of light-green coarse-grained tuffs with a vitroclastic texture. Intercalations of smaller bodies of medium- to fine-grained tuffs are present. Toward the southern part of the deposit, homogeneous fine-grained tuffs dominate the lithological succession; a general decrease in grain size

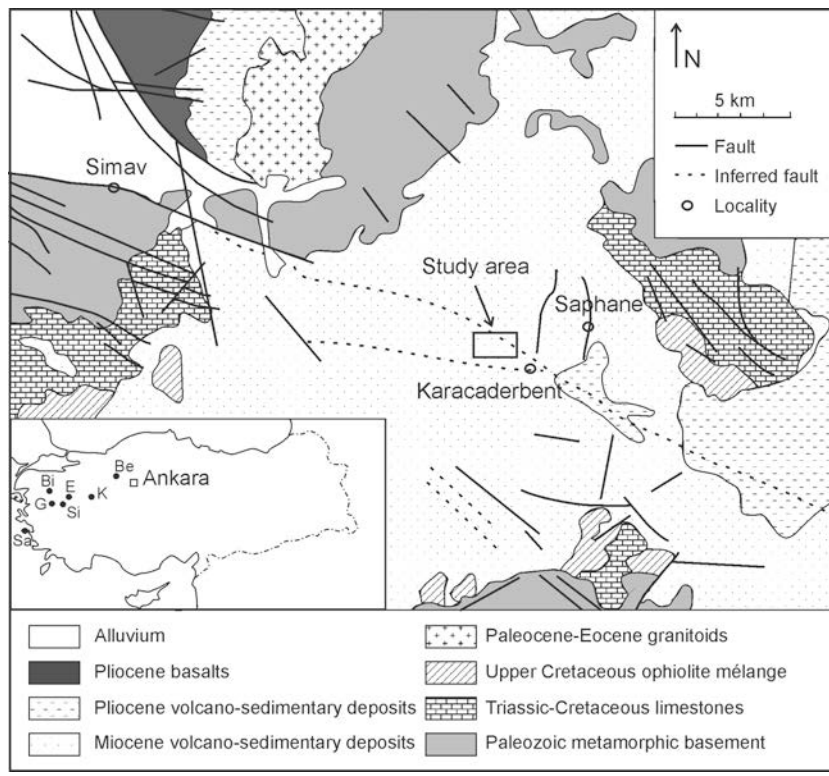

Figure 1. Simplified geological map of the central Simav graben (adapted from Oygür and Erler, 2000); inset indicates the location of the Simav graben (Si) and of the Beypazari (Be), Bigadiç (Bi), Emet (E), Kirka (K), Gördes (G), and Samos (Sa) zeolite occurrences.

https://doi.org/10.1346/CCMN.2008.0560603 Published online by Cambridge University Press

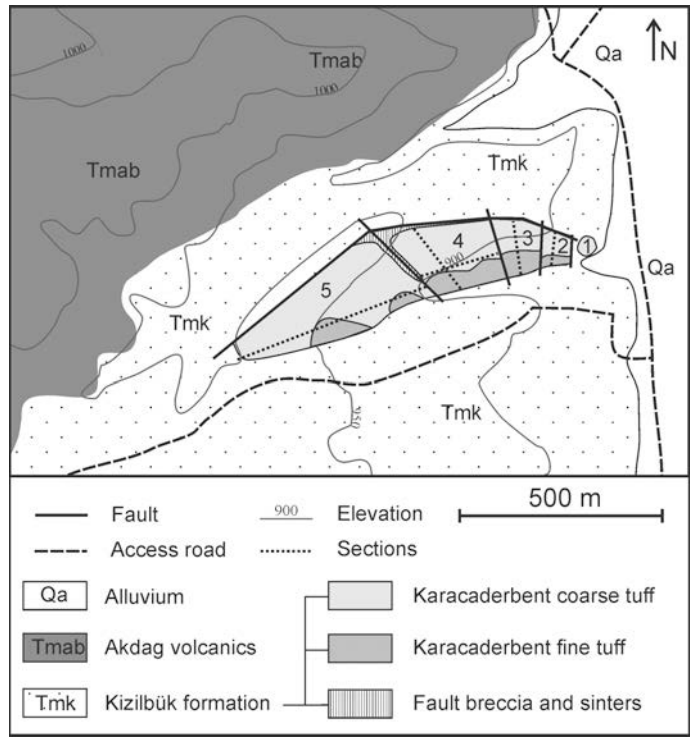

Figure 2. Detailed geological map of the Karacaderbent zeolite deposit. The extent of the brecciation zone is exaggerated for the purposes of clarity. The main sampled sections are indicated; additional samples were taken in the fault zones and randomly from block 5.

is noted from the north to the south, pointing to a source area in the north. The total thickness of the deposit is at least 30 m based on a vertical section, the base of the zeolite deposit could not be observed on location.

METHODS

Seventy samples from several sections through the tuff lens and adjacent lithologies were collected for investigation. Forty samples were then selected for further analysis by diverse methods; the selection was based on equal distribution along the defined sections. Sections were made according to the geometry of the tuff lens which is dissected by four N–S transform faults. The resulting blocks were sampled separately (Figure 2).

X-ray powder diffraction (XRPD) measurements for quantitative analysis were recorded on a Philips PW1830 device with CuKα radiation at 30 mA and 45 kV using a graphite monochromator. Diffractometer scans were recorded in Bragg-Brentano geometry from 5 to 70º2θ, with a step size of 0.02º2θ and 2 s per step. Prior to measurement, bulk samples were ground in a mortar to pass a 500 μm sieve, mixed with 10 wt.% ZnO as internal standard, and wet milled in methanol in a McCrone Micronising Mill® to obtain mean grain sizes of ~10 μm. Eventually, samples were side-loaded into aluminum holders for measurement. The XRPD data processing was carried out using the *Diffracplus* EVA® software for identification and the *Topas Academic*® software (Coelho, 2007) for Rietveld quantitative phase analysis (QPA) (Hill and Howard, 1987). To obtain more accurate quantitative results, a limited Rietveld structure refinement of the dominant clinoptilolite phase was needed. The population parameters of the various extra-framework cation sites were refined in order to obtain a better agreement between the structure model and the chemistry determined by electron microprobe analysis (EMPA). Rietveld refinement of minor phases started from literature structure models and involved least-squares fitting of global parameters such as zero-error and background, and phase-specific parameters such as scale factor, unit-cell dimensions, and profile parameters. In a limited number of samples the clay mineralogy was investigated by sedimentation of the dispersed <2 μm fraction, obtained by centrifugation (Moore and Reynolds, 1997), on a glass slide. To determine the presence of smectite, the samples were measured after air-drying and solvation with ethylene glycol on a Philips PW1130 with CoKα radiation (Ni-filter) at 20 mA and 30 kV.

Thin sections of the samples were examined using an optical microscope and C-coated rock chips were investigated using a scanning electron microscope (FEG XL30 (FEI)) at low acceleration voltages (10 kV) to limit beam damage. Polished, C-coated thin

https://doi.org/10.1346/CCMN.2008.0560603 Published online by Cambridge University Press

sections of selected samples were examined using an electron microprobe (Cameca SX50) equipped with wavelength-dispersive X-ray energy detectors. Measurements were carried out with an electron beam of 20 nA, 15 keV, and 25 μm^2 scanning beam spot. Counting times per set of three elements were 10 to 16 s. Measurements for the following elements were compared to appropriate mineral standards: Si, Al, Ca, Na, K, Mg, Fe, Ti, Mn, Sr, and Ba. ZAF corrections were applied. Analysis of pure clinoptilolite crystals were carried out in triplicate. Each time, a different location on the crystal was chosen in order to limit beam-damage effects.

The CEC values of the samples analyzed were determined following an ammonium acetate saturation procedure (AMAS) developed by Kitsopoulos (1999) specifically for natural zeolite samples.

The bulk chemistry was determined on glass beads that were made by fusing 3 g of sample and 8 g of flux (Li-tetraborate/metaborate) at 1100ºC. The glass beads were analyzed by X-ray fluorescence (XRF) spectroscopy using a Bruker SRS3400 (Bruker AXS, Karlsruhe, Germany). Trace element chemistry was measured on a Varian *Vista-MPX* inductively coupled plasma optical emission spectrometer (ICP-OES) system (Varian, Middelburg, the Netherlands). Mercury concentrations were determined by cold vapor atomic absorption spectrometry on a Hydra AA mercury analyzer (Teledyne Leeman Labs, Hudson, New Hampshire, USA).

RESULTS

Karacaderbent tuff member

The dominant lithology in the deposit is a coarse-grained lithified tuff consisting mainly of relict open-pumice fragments and bubble-wall glass shards randomly oriented in a light-green matrix; pumice fragment size ranges up to 5 cm. Pyrogenic crystals such as andesine, quartz, and biotite phenocrysts are present, accessory pyroxene and tourmaline were identified. The lithoclasts observed are collapsed pumice fragments and detrital particles derived from the metamorphic basement and surrounding Mesozoic to Paleogene lithologies as described in Figure 1. The overall pyrogenic minerals and lithoclasts content is <10% as determined by optical microscopy. Optical microscopy and SEM analysis revealed that the zeolitization process was preceded by the crystallization of a thin layer of yellow-brown smectite clay minerals on the surface of the pumice fragments and glass shards. As dissolution of the vitric phase proceeded, the formation and growth of microscopic tabular clinoptilolite and lepispheric to needle-shaped opal CT aggregates both inward and outward from this smectite outline followed (Figure 3). Eventually, clinoptilolite replaced glass shards and pumice fragments and also partially filled vugs and remaining pore space (Figure 4). In contrast, the collapsed pumice lithoclasts were replaced by a mixture of smectite and green celadonite minerals.

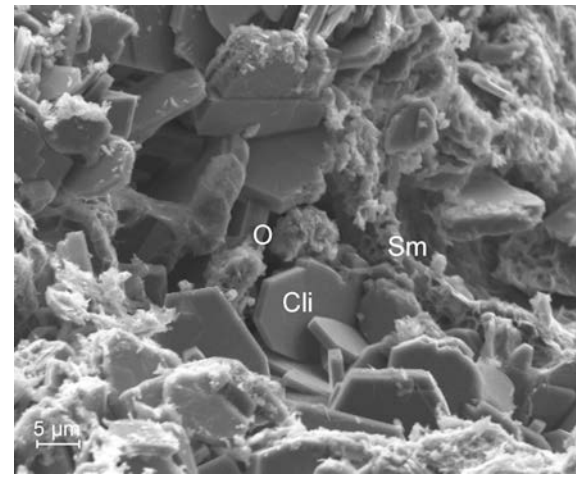

Figure 3. SEM image of the intergrowth of clinoptilolite (Cli), opal CT lepispheres (O), and smectite crystals (Sm).

Measurements by XRD of oriented sample mounts of the <2 µm fraction of air-dried and ethylene-glycol solvated samples (Figure 5) revealed shifts in basal spacings from 12.6 Å to 17.1 Å upon ethylene-glycol solvation, indicating the presence of smectite, and a smaller peak at 10.1 Å, indicating a minor amount of mica.

An example of bulk QPA by Rietveld refinement is given in Figure 6. The mineralogy of the coarse vitroclastic tuffs is dominated by clinoptilolite. Andesine, mica (celadonite and biotite as identified by electron microprobe analysis (EMPA) and microscopy), and quartz are present in smaller amounts; opal CT (cristobalite-tridymite) and calcite can be considered as accessory phases (Table 1). The QPA results indicate

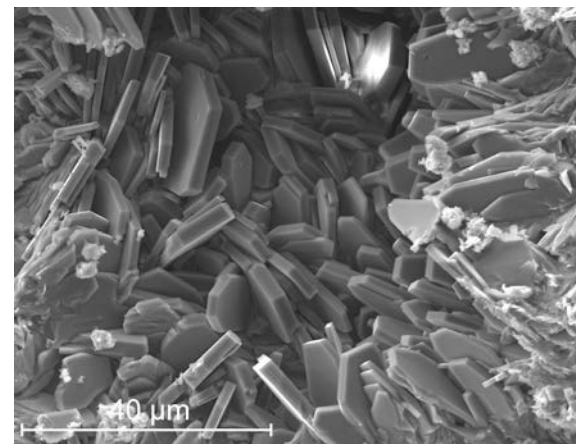

Figure 4. SEM image of characteristic 'coffin'-shaped clinoptilolite crystals grown in open pore space.

https://doi.org/10.1346/CCMN.2008.0560603 Published online by Cambridge University Press

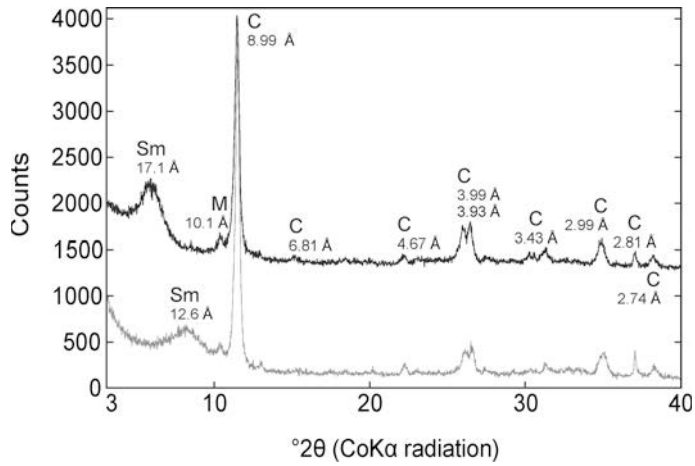

Figure 5. Representative XRD scan of the separated <2 μm fraction of the Karacaderbent tuff sedimented on a glass slide. In gray, below: XRD pattern of the air-dried sample; in black, above: the XRD pattern of the same sample after ethylene-glycol solvation. Apart from smectite (Sm) and mica (M), a significant amount of clinoptilolite (C) is present.

that the distribution in clinoptilolite content is very homogeneous (73−87 wt.%); fine-grained samples show less mineralogical variation than coarse-grained samples. No systematic lateral or vertical variations in mineralogy occur. Alkali-feldspar was encountered in samples close to the fault zones. In the fault zones, a degradation of the clinoptilolite content was observed. In sinters, alkali-feldspar and microsilica (mixture of opal CT and quartz) prevail, whereas no clinoptilolite was present.

Five samples were selected for microprobe analysis. The calculated structural formulae of the clinoptilolites analyzed are given in Table 2, the results were considered reliable when the chemical balance error function E% = $[(Al-Al_{theor})/Al_{theor}] \times 100$ was <10, where Al_{theor} = Na + K + 2(Ca + Mg + Sr +Ba) (Passaglia, 1970). Si/Al ratios ranged from 4.53 to 5.01 and a Si/Al ratio >4 suggests clinoptilolite (Coombs *et al.*, 1997). The dominant extra-framework cation was K (1.59−2.98), followed by Ca (1.02−1.80). The Mg content was found to be relatively constant in all analyses (0.48−0.70); Na contents were generally very small (0.02−0.22), but were observed to increase slightly toward the fault zones (0.27−0.40). The alkali/alkaline-earth ratios (A/AE) ranged between 0.80 and 1.92.

Pyrogenic plagioclase feldspars had a typical andesine−labradorite composition ($An_{40}-An_{60}$) and, toward the fault zones, authigenic alkali-feldspar associated with microsilica was encountered. Microprobe analyses of clay minerals, formed during early diagenetic alteration of glass shards, were biased by the extremely fine texture, which made prevention of matrix effects impossible. The intergrowth of smectite and microsilica resulted in an excessive Si content; however, the elevated Al and Fe contents indicate an Fe-rich smectite as observed by Gündogdu *et al.* (1996) in neighboring zeolite deposits. Celadonite was identified as an alteration product of collapsed pumice fragments. The celadonite structural formula points to an intermediate form between ferroaluminoceladonite ($KFe^{2+}AlSi_4O_{10}$

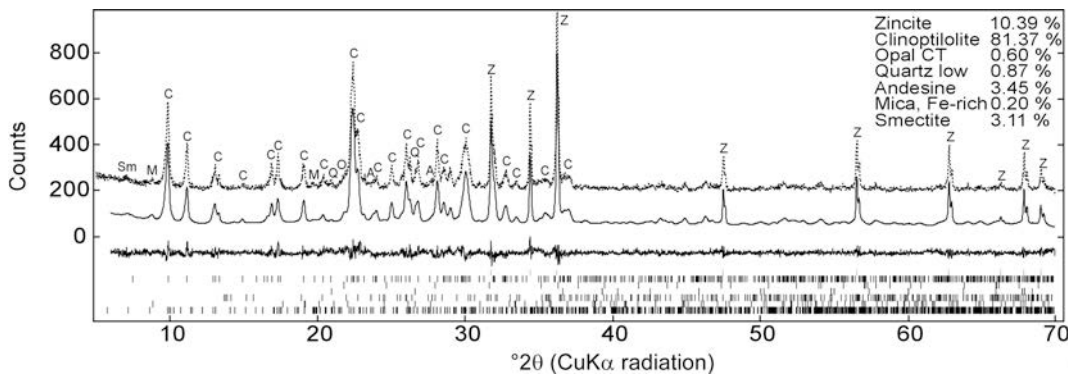

Figure 6. Rietveld refinement of a representative sample (fine-grained Karacaderbent tuff, block 5); 10 wt.% ZnO was added as internal standard. Above, the measured (dashed line) and calculated patterns (full line); underneath, the difference curve is given. Sm − smectite, M − mica, C − clinoptilolite, Q − quartz, O − opal CT, A − andesine, Z − zincite internal standard. Below, all reflection positions are presented of the phases given in the upper right corner.

https://doi.org/10.1346/CCMN.2008.0560603 Published online by Cambridge University Press

Table 1. Mineralogical composition determined by Rietveld refinement of XRPD data from samples of the Karacaderbent tuff. For fine-grained and coarse-grained tuffs, average and standard deviation values (SD) are reported.

Sample	Clinoptilolite	Opal CT	Quartz	Andesine	Mica	Smectite	Alkali feldspar	Calcite	Sum	Unidentified/ amorphous	Rwp (%)	GoF
Fine-grained tuff (N = 6)												
Average	84.20	0.60	0.98	4.83	0.46	3.87			94.94	5.10	16.20	1.26
SD	1.85	0.00	0.15	1.25	0.22	0.76				2.40	0.29	0.04
Coarse-grained tuff (N = 16)												
Average	82.53	0.54	0.94	7.81	1.01	4.31	0.94**	0.05*	98.06	2.15	16.32	1.28
SD	4.49	0.16	0.50	1.94	0.72	1.45	2.65	0.20		3.08	0.31	0.04
Fault-related												
Breccia block 3	43.4	7.5	1	21.3	3	4.6	18.7		99.5	0.5	15.54	1.27
Sinter		27.9	2.5	27.5	1.1		42.7	0.8	100	0	17.42	1.3

* Present in one sample.
** Present in two samples.

Table 2. Karacaderbent clinoptilolite composition determined by EMPA. The results are recalculated to 72 oxygen atoms. R = Si/(Si+Al), A/AE is the ratio of alkali over earth alkali elements. SD: standard deviation. E%: chemical balance error function (Passaglia, 1970).

Sample	Si	Al	Fe	Ca	Mg	Na	K	Sr	Ba	Si/Al	R	A/AE	E%
Fine-grained tuff (N = 5)													
Average	29.65	6.38	0.01	1.24	0.53	0.35	2.05	0.09	0.05	4.65	0.82	1.35	2.22
SD	0.05	0.07	0.01	0.09	0.01	0.08	0.11	0.01	0.02	0.05	0.00	0.05	5.65
Coarse-grained tuff (N = 13)													
Average	29.76	6.21	0.01	1.30	0.56	0.11	2.16	0.10	0.04	4.80	0.83	1.28	-0.74
SD	0.18	0.12	0.01	0.24	0.07	0.04	0.47	0.01	0.03	0.12	0.00	0.45	6.26

$(OH)_2$) and celadonite ($KMgFe^{3+}Si_4O_{10}(OH)_2$) (Li *et al.*, 1997). In one sample, dolomite rhombohedra were found in association with clinoptilolite.

Exchangeable cations were released by NH_4 exchange and measured CEC values ranged from 191 to 208 meq/100 g (Table 3). The CEC values were smaller in the fault zones (132 meq/100 g) and fine- and coarse-grained facies were not significantly different. The overall CEC values were close to the calculated values for an 80−85 wt.% pure clinoptilolite tuff, when a CEC value of 240 meq/100 g for pure clinoptilolite was assumed (Breck, 1974). The cations released by NH_4 exchange were dominated by K and Ca with lesser amounts of Na and Mg. The K/Ca and K/Mg ratios obtained by NH_4 exchange were similar to the values obtained by EMPA. However, a consistent deviation was observed in the K/Na ratios. The Na released in the CEC tests was greater than that measured by EMPA. This can partially be explained by the contribution of smectite to the CEC. Small amounts of Na in smectite, determined by EMPA, nonetheless suggest that some migration and volatilization of alkali occurred in the electron microprobe beam.

The XRF analysis results of fine- and coarse-grained zeolitic tuffs indicated large SiO_2, Al_2O_3, and K_2O contents, whereas the Fe_2O_3, CaO, Na_2O, MgO, BaO, and SrO contents were small (Table 4). The overall compositional variation was very little in the fine-grained tuff samples. Coarse-grained tuffs showed somewhat greater variability, mainly in exchangeable cations. A negative correlation between the K_2O and CaO contents indicates exchange of K for Ca and *vice versa*. The largest relative variation was in the Na_2O. Greater Na_2O contents were observed for zeolite samples near fault zones. Overall loss on ignition (LOI) values were large (~13 wt.%) and consistent with the high zeolite content determined by QPA Rietveld refinement. The Si/Al ratios in the bulk samples were somewhat greater than the ratios determined by EMPA for clinoptilolite and suggest the presence of silica-rich phases, such as quartz and opal CT. Toxic trace element levels were small in the main tuff body (Table 4).

Fault-related breccia and sinters

The fault zones dividing the deposit into several blocks contain silicified breccia and sinters. Intrusion of silica-rich fluids along the transform faults into the tuff body caused intensive brecciation of the tuffs and cementation of the breccia fragments in a siliceous matrix (opal CT, quartz). Sinters are located in the center of the broader fault zones and consist of quartz-filled vesicles set in a dark-colored matrix mainly composed of microsilica, authigenic alkali feldspar, and plagioclase phenocrysts. Infilling of pore space and partial replacement of zeolites by blue-greenish clay minerals occurred along the fault zones. Variations in intensity of solid-fluid interaction presumably resulted in the formation of the cm-wide blue and ochre bands.

The Rietveld QPA indicated significantly decreased clinoptilolite and increased microsilica contents toward the fault zones (Table 1). Clinoptilolite was absent from the sinters and opal CT was the dominant silica phase in the breccia and the sinters. The alkali feldspar content increased toward the fault zone. Additionally, a considerable amount of plagioclase was present.

Electron microprobe measurements on the sinter revealed the presence of both authigenic Na- and K-rich feldspars. The composition of the plagioclase phenocrysts is identical to the plagioclase composition in the zeolitized tuff (An_{40}−An_{60}).

The CEC values of the silicified breccia were smaller by the same extent as the decreased zeolite contents were with respect to the zeolitized tuff (Table 3). The amounts of Na and Mg released from the zeolitized tuff were less than the main tuff body.

The results from the XRF analyses (Table 4) show that fault-related breccia and sinters contained greater amounts of SiO_2 and Na_2O, and had smaller LOI values compared to the Karacaderbent tuff. The very small LOI values measured in some samples indicate that only very small amounts of hydrous phases were present. In

Table 3. Averages and standard deviation values (SD) of CEC analyses of representative samples from the Karacaderbent tuff.

Sample	Released Ca (meq/100 g)	Released Mg (meq/100 g)	Released Na (meq/100 g)	Released K (meq/100 g)	CEC (meq/100 g)
Fine-grained tuff (N = 3)					
Average	86.04	16.07	24.37	59.47	202.00
SD	13.05	1.09	1.31	9.48	6.63
Coarse-grained tuff (N = 9)					
Average	89.51	11.76	30.28	62.32	197.75
SD	21.94	4.18	8.12	9.32	5.72
Fault-related					
Block 3	78.84	4.51	3.29	40.79	131.96

https://doi.org/10.1346/CCMN.2008.0560603 Published online by Cambridge University Press

Table 4. Chemical composition of representative tuffs from the Karacaderbent tuff based on XRF analyses. SD is standard deviation. LOI values are determined by heating at 1050ºC for 2 h.

Sample	Fine-grained tuff (N = 3)		Coarse-grained tuff (N = 9)		Fault-related		
(wt.%)	average	SD	average	SD	Block 3	Breccia block 3	Sinter
SiO_2	65.13	0.67	64.97	1.25	67.10	64.50	76.60
Al_2O_3	12.37	0.21	12.97	0.47	13.20	13.60	12.20
TiO_2	0.20	0.00	0.22	0.02	0.21	0.24	0.21
Fe_2O_3	1.15	0.09	1.36	0.15	1.28	1.36	0.70
MnO	0.01	0.00	0.03	0.06	0.01	0.02	0.05
MgO	0.53	0.39	0.90	0.18	0.72	0.85	0.10
CaO	2.24	0.22	2.51	0.48	2.03	2.29	1.11
K_2O	3.64	0.07	3.83	0.55	4.61	3.39	3.99
Na_2O	0.89	0.26	0.90	0.72	1.00	1.89	3.22
BaO	0.22	0.02	0.20	0.04	0.22	0.19	0.19
SrO	0.08	0.00	0.06	0.02	0.04	0.06	0.03
P_2O_5	0.015	0.004	0.029	0.013	0.017	0.030	0.025
Cr_2O_3	0.002	0.000	0.003	0.001	0.002	0.003	0.012
LOI	13.25	0.15	12.01	2.16	9.60	11.53	1.50
(ppm)							
Pb	27.60	22.92	26.98	20.91	45.00	36.00	7.80
As	1.23	0.23	4.94	10.18	6.60	4.80	15.00
Cd	0.31	0.05	0.55	0.40	0.73	0.65	0.54
F	14.00	4.36	26.67	15.95	17.00	26.00	24.00
Hg	0.001	0.000	0.008	0.009	0.030	0.008	0.005
Sum	99.73		99.99		100.04	99.95	99.94
Si/Al	5.27	0.14	5.02	0.18	5.08	4.74	6.28
A/EA	1.49	0.14	1.37	0.56	1.86	1.56	5.04

addition, substantially smaller amounts of MgO, Fe_2O_3, and CaO were present in the sinter. Arsenic concentrations were found to be slightly greater in the sinter phase. No other toxic trace element levels in fault-related lithologies differed significantly from the concentrations in the main tuff.

DISCUSSION

Pre-alteration materials

A comparison of the Karacaderbent tuff chemistry with neighboring, unaltered tephra and tuff deposits of similar age can yield important information about the zeolitization environment. Overall changes in chemistry can reveal the interaction of unaltered vitreous material with pore fluids. In Table 5, the chemical composition of the Karacaderbent tuff, recalculated on an anhydrous basis, is compared to the chemistry of nearby Middle Miocene unaltered tephra from the Köpenez formation (Emet basin) (Gündogdu *et al.*, 1996), 20 km northeast of Karacaderbent, and from the Middle Miocene Civanadag tuff (Mutlu *et al.*, 2005), 4 km east of Karacaderbent. The glass and unaltered tuff samples have large K_2O and SiO_2 values and are identified as rhyolitic in composition (Le Bas *et al.*, 2003). The small Al_2O_3 and Fe_2O_3 values support this classification, because Al and Fe are considered to be immobile elements (Fisher and Schmincke, 1984). The very similar composition of the Karacaderbent tuff indicates that the pre-alteration materials were K-rich and rhyolitic. Noteworthy differences between the unaltered materials and the zeolitized material are observed mainly in the Fe_2O_3 content which was slightly greater in the zeolitized tuffs and in the amounts of alkali and alkaline earth elements. The amounts of CaO and MgO were invariably greater in the zeolitized material. The K_2O content was greater in the unaltered materials. The Na_2O content of the Civanadag tuff was also greater than that of the Karacaderbent tuff or the Köpenez tephra. These observations indicate considerable mobility of alkalis during zeolitization of the tuff. During zeolitization, Ca and Mg were taken up and K and Na were released.

Based on the distribution of sedimentary facies, Gündogdu *et al.* (1996) noted that the Middle Miocene zeolitized tuffs of the Köpenez Formation originated southwest of the Emet basin. The presence of petrographically and chemically similar volcano-sedimentary lithologies in the central Simav graben with a source area situated to the north supports this view and points to an identical volcanic source for the Köpenez and Karacaderbent tuffs.

Zeolitization environment

The presence in the Aegean (western Turkey, southern Serbia and Samos Island) of extensive zeolite deposits which were formed in saline-alkaline lake environments in the middle to late Miocene (Gottardi

https://doi.org/10.1346/CCMN.2008.0560603 Published online by Cambridge University Press

Table 5. Comparison table of average chemical compositions and standard deviation values (SD) recalculated on an anhydrous basis of the Köpenez tephra (Semelin, 1985, in Gündogdu *et al.*, 1996), the Civanadag tuff (Mutlu *et al.*, 2005), the Karacaderbent tuff, and the Köpenez tuff (Semelin, 1985, in Gündogdu *et al.*, 1996).

Sample	Facies	SiO_2	Al_2O_3	TiO_2	Fe_2O_3	MgO	CaO	K_2O	Na_2O
Köpenez tephra (N = 6)									
Average		75.39	14.13	0.15	1.09	0.13	0.98	6.86	1.17
SD		0.90	0.67	0.06	0.16	0.05	0.18	0.36	0.39
Civanadag tuff (N = 3)									
Average		74.22	14.07	0.27	1.17	0.50	0.73	6.07	2.51
SD		1.14	0.90	0.02	0.56	0.28	0.39	0.80	1.76
Karacaderbent tuff (N = 12)									
Average	K-clinoptilolite + opal CT	74.21	14.63	0.25	1.49	0.92	2.79	4.32	1.02
SD		1.27	0.57	0.03	0.18	0.32	0.50	0.54	0.71
Köpenez tuff	Glass + smectite	75.72	13.86	0.22	1.76	0.6	1.38	5.23	1.22
	K-clinoptilolite + opal-CT	76.15	14.02	0.24	1.56	0.97	2.48	3.94	0.64
	Ca-clinoptilolite + K-feldspar + quartz	75.67	14.31	0.23	1.49	1.1	4.12	2.81	0.27
	K-feldspar + analcime + smectite + quartz	77.97	11.55	0.18	0.83	0.25	1.46	5.07	2.7

and Obradovic 1978; Helvaci *et al.*, 1993; Gündogdu *et al.*, 1996; Stamatakis *et al.*, 1996; Esenli and Sirkecioglu, 2005) suggests that zeolitization of the Karacaderbent tuff took place in similar, mildly to highly saline-alkaline basins. However, evidence of extensive hydrothermal activity along the Simav graben and even in the Karacaderbent tuff could point to zeolitization caused by hydrothermal fluids infiltrating through faults and fissures.

Mutlu *et al.* (2005) concluded that the alunite ore deposit near Saphane was formed under strongly acidic conditions with an important base-metal leaching of wall rocks. The transformation of host rock to alunite was accompanied by the release of silica and resulted in the extensive silicification of the surrounding tuffaceous host rock along transform faults. Oygür (1997) reported similar mechanisms involving the formation of Hg/Au/Ag deposits at Mumcu and of the Sb deposit at Degirmenciler (Oygür and Erler, 1999), both situated west of Simav along the Simav graben. The Karacaderbent tuff has also been affected by hydrothermal activity with associated brecciation and silicification along transform faults.

Several arguments can be formulated against a hydrothermal zeolitization process. First of all, the fluid compositions responsible for the formation of the different ore bodies along the Simav graben were strongly acidic in composition (Mutlu *et al.*, 2005). This is incompatible with zeolite alteration which occurs under mildly alkaline conditions (Sheppard and Hay, 2001). Second, a breakdown of clinoptilolite was observed in the direction of the fault zones, while sinters did not contain any zeolites. Third, the homogeneity of the deposit is not typical of hydrothermal zeolitization (Utada, 2001). Fourth, no high-temperature zeolites occur near the fault zones. Fifth, near the fault zones, changes in clinoptilolite extra-framework cations without changes in framework composition suggest that clinoptilolite composition was altered by infiltrating fluids originating in the fault zones. The intense brecciation of lithified material in the fault zones suggests that lithification and thus zeolitization preceded hydrothermal activity.

From differences in chemistry of the diagenetic facies, four facies in the Köpenez Formation (Emet basin) were distinguished and related to increasing lacustrine water alkalinity and salinity, and to rock porosity (Table 5) (Gündogdu *et al.*, 1996). Diagenetic alteration to smectite glass occurred in Ca- and Mg-rich solutions of low alkalinity and salinity. An increase in alkalinity associated with minor solid-fluid interaction resulted in the formation of K-clinoptilolite and opal CT. A more intensive solid-fluid interaction resulted in the formation of Ca-clinoptilolite associated with K-feldspar. Even greater salinities were invoked to explain the diagenetic alteration to K-feldspar and analcime-dominated authigenic mineralogy (Gündogdu *et al.*, 1996). The presence of borates at the top of the Miocene sedimentary sequence in the Emet basin supports their argument. Very similar distributions of diagenetic facies were reported from other zeolite occurrences in saline-alkaline basins in the Aegean (Helvaci *et al.*, 1993; Gündogdu *et al.*, 1996). A comparison of the Karacaderbent tuff chemistry and mineralogy with the K-clinoptilolite facies of the Köpenez Formation shows nearly identical compositions and supports the hypothesis that both originated from the same material and that the zeolitization processes were similar.

In the Karacaderbent tuff, the association of calcite, dolomite, K-clinoptilolite, and the greater amounts of Ca and Mg present in clinoptilolite compared to probable

https://doi.org/10.1346/CCMN.2008.0560603 Published online by Cambridge University Press

unaltered starting materials (Table 5) suggest that the zeolitizing fluids were rich in Ca and Mg, derived from surrounding carbonate lithologies. It is assumed that pH was controlled by the calcite or dolomite precipitation product. No typical evaporitic minerals or authigenic K-feldspar were identified, indicating that salinities during zeolitization were relatively low and pH <9 (Surdam and Parker, 1972). Further, a calculation of fluid chemistry using the method proposed by Boles and Surdam (1979) based on the clinoptilolite cation fractionation in deep-sea sediments gave the following values for K/Na/Ca/Mg proportions in the fluid: 1/4/37/17. Extrapolating the results of Jones (1965) (in Boles and Surdam, 1979), the log((Na+K)/(Ca+Mg)) value gave an estimate of the amount of total dissolved solids in the fluid of ~180 ppm, suggesting dilute pore solutions.

Although zeolitization in an open hydrologic system, where the distribution of diagenetic alteration facies follows the path of the percolating fluids (Langella *et al.*, 2001), cannot be completely excluded due to the limited thickness of the deposit accessible at the outcrop, the presence of both early-formed (smectite lining relict glass shards) and late-formed (clinoptilolite and opal CT) diagenetic alteration products suggests diagenetic alteration in a closed hydrologic system (Hay and Sheppard, 2001). Zeolitization of rhyolitic glass results in the release of excess silica (Boles and Coombs, 1975). The close association of opal CT and clinoptilolite with a large Si/Al ratio suggests that this silica was not removed from the system.

The present argument suggests that zeolitization took place under relatively low-salinity conditions in a closed hydrologic system in a lacustrine environment. Whether the Karacaderbent tuff could be situated in the periphery of a larger saline-alkaline lake or whether salinities and alkalinities did not reach greater levels due to graben infill by the deposition of the unzeolitized overlying Middle Miocene Civanadag tuff and Akdag volcanics, remains unclear.

Potential applications

In 2006, Turkish zeolite production totalled 35,000 tons of which 80% was used for the domestic market. Of the rest, exports were mainly to the USA, France, Italy, Israel, the Netherlands, Spain, and the United Kingdom. Domestic and foreign demands were increasing. Uses in fertilizer, as a soil conditioner, and in water-treatment applications represented the most important domestic markets. Globally, the most important applications of natural zeolites were in the construction industry, agriculture, animal feed, and waste-water treatment (Virta, 2006).

This work revealed interesting perspectives for exploitation and application of the Karacaderbent zeolite deposit. Beneficial characteristics are the large-scale homogeneity and large clinoptilolite content. The high K/Na ratio and elevated CEC values would permit applications in agriculture and aquaculture (Polat *et al.*, 2004), for potable and waste-water treatment (Esenli and Sirkecioglu, 2005), and in the immobilization of radioactive elements (Mumpton, 1999). Moreover, the levels of toxic trace elements are below EU specifications for use as a feed additive (Directive 2002/32/EC). In the construction industry, both high- and low-quality zeolite materials can be used for supplementary cementing material in high-performance concrete (Chan and Yi, 1999) and in aggregates or pozzolans in blended cements (Akman *et al.*, 1992), respectively.

SUMMARY AND CONCLUSIONS

An extensive mineralogical and chemical characterization of the zeolitized Karacaderbent tuff was performed. A mineralogical and geochemical comparison with neighboring zeolite deposits suggested that rhyolitic K-rich tephra was zeolitized to K-clinoptilolite in a closed hydrologic system under low-salinity conditions. The zeolitization process preceded a hydrothermal event which had only a minor influence on zeolite chemistry along the fault zones.

The elevated zeolite content and CEC, low levels of toxic trace elements, and the deposit homogeneity demonstrated the possible economic value of the Karacaderbent tuff.

ACKNOWLEDGMENTS

The authors thank Herman Nijs for preparation of thin sections, Jacques Wautier for assistance with the microprobe analyses, and Danny Coetermans for help with the CEC measurements. The reviewers Dr Ursula Kelm, Dr Elio Passaglia, and Dr Michael Stamatakis and the Associate Editor are gratefully acknowledged for their significant contributions to the manuscript. The first author and Gilles Mertens were recipients of the Flemish Fund for Scientific Research (FWO).

REFERENCES

Akman, M.S., Mazlum, F., and Esenli, F. (1992) A comparative study of natural pozzolans used in blended cement production. *ACI Special Publication*, **32**, 471–494.

Boles, J.R. and Coombs, D.S. (1975) Mineral reactions in zeolitic Triassic tuff, Hokonui Hills, New Zealand. *Bulletin of the Geological Society of America*, **86**, 163–173.

Boles, J.R. and Surdam, R.C. (1979) Diagenesis of volcanogenic sediments in a Tertiary saline lake: Wagon Bed Formation, Wyoming. *American Journal of Science*, **111**, 832–853.

Bozkurt, E. (2001) Late Alpine evolution of the Central Menderes Massif, western Turkey. *International Journal of Earth Sciences*, **89**, 728–744.

Breck, D.W. (1974) *Zeolite Molecular Sieves: Structure, Chemistry, and Use*. John Wiley and Sons, New York, 771 pp.

Chan, S.Y. and Yi, X. (1999) Comparative study of the initial surface absorption and chloride diffusion of high performance zeolite, silica fume and PFA concretes. *Cement & Concrete Composites*, **21**, 293–300.

Coelho, A.A. (2007) Topas-Academic. http://members.optusnet.com.au/alancoelho/.

Coombs, D.S., Alberti, A., Armbruster, T., Artioli, G., Colella, C., Galli, E., Grice, J.D., Liebau, F., Mandarino, J.A., Minato, H., Nickel, E.H., Passaglia, E., Peacor, D.R., Quartieri, S., Rinaldi, R., Ross, M., Sheppard, R.A., Tillmans, E., and Vezzalini, G. (1997) Recommended nomenclature for zeolite minerals: Report of the subcommittee on zeolites of the International Mineralogical Association, Commission on New Minerals and Mineral names. *The Canadian Mineralogist*, **35**, 1571–1606.

Esenli, F. and Sirkecioglu, A. (2005) The relationship between zeolite (heulandite–clinoptilolite) content and the ammonium-exchange capacity of pyroclastic rocks in Gördes, Turkey. *Clay Minerals*, **40**, 557–564.

Fisher, R.V. and Schmincke, H.-U. (1984) *Pyroclastic Rocks*. Springer-Verlag, Berlin, 472 pp.

Gottardi, G. and Obradovic, J. (1978) Sedimentary Zeolites in Europe. *Fortschritte der Mineralogie*, **56**, 316–366.

Gündogdu, M.N., Yalçin, H., Temel, A., and Clauer, N. (1996) Geological, mineralogical and geochemical characteristics of zeolite deposits associated with borates in the Bigadiç, Emet and Kirka Neogene lacustrine basins, western Turkey. *Mineralium Deposita*, **31**, 492–513.

Hay, R.L. and Sheppard, R.A. (2001) Occurrences of zeolites in sedimentary rocks: an overview. Pp 217–234 in: *Natural Zeolites: Occurrence, Properties, Applications* (D.L. Bish and D.W. Ming, editors). Reviews in Mineralogy and Geochemistry **45**, Mineralogical Society of America and the Geochemical Society, Washington D.C.

Helvaci, C., Stamatakis, M.G., Zagouroglou, C. and Kanaris, J. (1993) Borate minerals and related authigenic silicates in northeastern Mediterranean late Miocene continental basins. *Exploration and Mining Geology*, **2**, 171–178.

Hill, R.C and Howard, C.J. (1987) Quantitative phase analysis from neutron powder diffraction data using the Rietveld method. *Journal of Applied Crystallography*, **20**, 467–474.

Jones, B.F. (1965) The hydrology and mineralogy of Deep Springs Lake, Inyo County, California. *U.S. Geological Survey Professional Paper* **502-A**, 56 pp.

Kitsopoulos, K.P. (1999) Cation-exchange capacity (CEC) of zeolitic volcaniclastic materials: applicability of the ammonium acetate (AMAS) method. *Clays and Clay Minerals*, **47**, 688–696.

Langella, A., Cappelletti, P., and de' Gennaro, M. (2001) Zeolites in closed hydrologic systems. Pp. 252–257 in: *Natural Zeolites: Occurrence, Properties, Applications* (D.L. Bish and D.W. Ming, editors). Reviews in Mineralogy and Geochemistry **45**, Mineralogical Society of America, and the Geochemical Society, Washington D.C.

Le Bas, M.J., Le Maitre, R.W., Streckeisen, A., and Zanettin, B. (2003) A chemical classification on the total alkali-silica diagram. *Journal of Petrology*, **27**, 745–750.

Li, G., Peacor, D.R., Coombs, D.N., and Kawachi, Y. (1997) Solid solution in the celadonite family: the new minerals ferroceladonite $K_2Fe_2^{2+}Fe_2^{3+}Si_8O_{20}(OH)_4$, and ferroaluminoceladonite, $K_2Fe_2^{2+}Al_2Si_8O_{20}(OH)_4$. *American Mineralogist*, **82**, 503–511.

Moore, D.M. and Reynolds, C.R. (1997) *X-ray diffraction and the Identification and Analysis of Clay Minerals*. Oxford University Press, New York, 378 pp.

Mumpton, F.A. (1999) La roca magica: Uses of natural zeolites in agriculture and industry. *Proceedings of the National Academy of Science USA*, **96**, 3463–3470.

Mutlu, H., Sariiz, K., and Kadir, S. (2005) Geochemistry and origin of the Saphane alunite deposit, Western Anatolia, Turkey. *Ore Geology Reviews*, **26**, 39–50.

Oygür, V. (1997) Anatomy of an epithermal mineralization: Mumcu (Balikesir-Sindirgi), Inner Western Anatolia, Turkey. *Mineral Research Exploration Bulletin*, **119**, 29–39.

Oygür, V. and Erler, A. (1999) Comparison of the epithermal and base-metal mineralizations along the Simav graben. Pp. 12–13 in: *Proceedings of the 52nd Geological Congress of Turkey, May 1999*, *Ankara* (in Turkish with English abstract).

Oygür, V. and Erler, A. (2000) Metallogeny of the Simav graben (Inner-Western Anatolia, Turkey). *Geological Bulletin of Turkey*, **43**, 7–19.

Passaglia, E. (1970) The crystal chemistry of chabazites. *American Mineralogist*, **55**, 1278–1301.

Polat, E., Karaca, M., Demir, H., and Onus N.A. (2004) Use of natural zeolite (clinoptilolite) in agriculture. Pp. 183–189 in: *Orchard Management in Sustainable Fruit Production*. *Journal of Fruit and Ornamental Plant Research*, special ed. vol. 12.

Purvis, M. and Robertson, A. (2005) Miocene sedimentary evolution of the NE–SW trending Selendi and Gördes basins, Western Turkey: implications for extensional processes. *Sedimentary Geology*, **174**, 31–62.

Seyitoglu, G., Anderson, D., Nowell, G., and Scott, B. (1997) The evolution from Miocene potassic to Quaternary sodic magmatism in western Turkey: implications for enrichment processes in the lithospheric mantle. *Journal of Volcanology and Geothermal Research*, **76**, 127–147.

Sheppard, R.A. and Hay, R.L. (2001) Formation of zeolites in open hydrologic systems. Pp. 261–276 in: *Natural Zeolites: Occurrence, Properties, Applications* (D.L. Bish and D.W. Ming, editors). Reviews in Mineralogy and Geochemistry **45**, Mineralogical Society of America and the Geochemical Society, Washington D.C.

Stamatakis, M.G. (1989) Authigenic silicates and silica polymorphs in the Miocene saline-alkaline deposits of the Karlovassi basin, Samos, Greece. *Economic Geology*, **84**, 788–798.

Stamatakis, M.G., Hall, A., and Hein, J.R. (1996) The zeolite deposits of Greece. *Mineralium Deposita*, **31**, 473–481.

Surdam, R.C. and Parker, R.D. (1972) Authigenic aluminosilicates minerals in the tuffaceous rocks of the Green River Formation, Wyoming. *Geological Society of America Bulletin*, **83**, 689–700.

Utada, M. (2001) Zeolites in hydrothermally altered rocks. Pp. 305–310 in: *Natural Zeolites: Occurrence, Properties, Applications* (D.L. Bish and D.W. Ming, editors). Reviews in Mineralogy and Geochemistry **45**, Mineralogical Society of America and the Geochemical Society, Washington D.C.

Virta, R.L. (2006) Zeolites. *U.S. Geological Survey Minerals Yearbook 2006*. http://minerals.usgs.gov/minerals/pubs/commodity/zeolites/zeolimyb06.pdf

(*Received 14 March 2008; revised 9 August 2008; Ms. 0144; A.E. W. Jaynes*)